DATA PROCESSING AND CONDITIONING FOR COMPARISON OF ACCELERATION SIGNALS FROM GNSS AND IMU READINGS

Marcos Espindola[1,2]; Paulo Kurka[2]

[1]Federal Institute of São Paulo, IFSP — Brazil
[2]School of Mechanical Engineering, FEM/UNICAMP — Brazil

ABSTRACT

This paper presents a comprehensive methodology for synchronizing and benchmarking raw Inertial Measurement Unit (IMU) acceleration signals against accelerations derived from Global Navigation Satellite System (GNSS) position data. The proposed approach is designed for railway track quality assessment and rolling stock verification, combining the absolute spatial precision of GNSS with the high-resolution, localized dynamic data provided by triaxial accelerometry. A core challenge in multi-sensor railway monitoring involves the reconciliation of disparate sampling rates, distinct frames of reference, and inherent sensor-specific noise. To address this, the methodology employs signal conditioning techniques, including resampling algorithms and coordinate transformation operations, to enable a reliable comparison between instruments operating under real-world conditions. The study introduces a data-processing framework that may be used to the identification of mechanical wear on rails and wagons, as well as detecting track geometry disturbances. The results are validated against an open-access experimental reference dataset and demonstrate that signal conditioning and frames of reference alignment are essential prerequisites for effective multi-sensor data fusion. The findings confirm the framework's ability to provide physically grounded insights, offering a transparent alternative to "black-box" analytical models in complex railway environments.

Keywords: *Railway sensors data processing; GNSS; IMU; Inertial odometry; Digital signal processing;*

1. INTRODUCTION

Effective railway infrastructure management necessitates continuous monitoring of track geometry and rolling stock health to uphold operational safety, passenger comfort, and cost-efficiency (Orbán; Gocica; Mărculescu, 2024; Yalınız; İça, 2020). To meet these demands, modern operators increasingly deploy instrumented vehicles that collect high-density data during regular service (Judek et al., 2022; Chen et al., 2018). These systems typically integrate Global Navigation Satellite Systems (GNSS) for spatial localization with Inertial Measurement Units (IMU) to capture rail dynamics and track irregularities through multi-axis accelerometers and gyroscopes (Zhou et al., 2025; González-Carbajal et al., 2022; Chen et al., 2015).

While the fusion of GNSS and IMU data offers significant potential for infrastructure evaluation, it remains technically demanding. Commercially available GNSS units generally provide localization precision within a few meters (Chen et al., 2015; Kumar, 1988). Conversely, IMU sensors capture high-frequency dynamic responses, often exceeding $100\ Hz$ enabling the detection of localized defects such as rail wear, curvature transitions, and terrain disturbances (Xie; Chen, 2024; Chen et al., 2015).

A critical challenge arises because these systems often operate with disparate sampling rates, distinct frames of reference, and differing physical measurement principles, complicating direct data integration and comparative analysis (Espindola; Kurka, 2026; Zhou; Yang; Hecht, 2023).

The central motivation of this study lies in addressing a fundamental challenge in multi-sensor railway monitoring: achieving synchronization and reliable comparison of data collected under variable operating conditions. The inherent discrepancies in temporal and spatial resolutions between GNSS and IMU systems demand rigorous resampling and time-alignment procedures. Without systematic signal conditioning, correlating GNSS derived track geometry with IMU measured dynamic responses remains problematic, thereby constraining the development of comprehensive track databases and the validation of maintenance interventions. (Zhou et al., 2025; Chen et al., 2015).

While Machine Learning (ML) and Artificial Intelligence (AI) offer powerful pattern recognition and adaptive capabilities, they introduce significant technical vulnerabilities. These include a heavy dependency on high-fidelity datasets, limited interpretability, often referred to as the "black box" nature of deep neural networks, and the requirement for extensive retraining when encountering new operating conditions. Furthermore, automated ML pipelines may produce statistically plausible results that nonetheless violate fundamental physical principles or ignore sensor constraints. Consequently, there is a growing trend toward integrating AI with classical digital signal processing to ensure that data-driven insights remain physically grounded and transparent (Hadj-Mabrouk, 2026; Pires; Santos; Junior, 2023).

In this context, this article contributes by introducing a signal processing approach that enables multi-sensor cross-validation. The proposed novelty lies in aligning the IMU accelerometer coordinate system with a reference frame derived from GNSS data. This procedure, not previously reported in the literature, ensures consistency between heterogeneous measurement sources and enhances the reliability of subsequent analyses. The specific objectives are as follows:

- Establish signal processing algorithms that convert discrete GNSS position data into continuous acceleration signals comparable with raw IMU measurements.
- Implement procedures to harmonize disparate sampling rates, align distinct coordinate systems, and mitigate sensor-specific noise characteristics.
- Demonstrate the robustness of the methodology through a practical case study.

The proposed framework is validated using an open-access reference dataset for rail vehicles (Winter, 2020), which provides a standardized baseline to assess the performance, accuracy, and reliability of the developed algorithms.

The remainder of this paper is organized as follows: Section 2 describes the signal processing methodology used; Section 3 describes the dataset used and the results of applying the proposed technique and Section 4 concludes with key findings and future research directions.

2. METHODOLOGY

The proposed methodology establishes a deterministic link between the discrete spatial coordinates provided by the GNSS and the high-frequency dynamic responses captured by the IMU. The workflow is designed to resolve the inherent discrepancies in sampling rates and reference frames through a sequence of kinematic derivations and linear transformations.

The proposed processing architecture is partitioned into four primary stages, beginning with the acquisition of raw GNSS and IMU data from the validated reference dataset established by (Winter, 2020). The primary data vectors are then processed through a conditioning resampling and temporal synchronization to establish a uniform time base. Subsequently, reference acceleration profiles are derived from GNSS data using kinematic vectors. The final stage involves a correlation-based inertial alignment, which synchronizes the raw IMU acceleration with the GNSS-derived reference to ensure spatial and temporal consistency across the integrated system. Description of the implementing stages are shown in Table 1. Similar strategies of data pre-processing and purging are present in (Zhou et al., 2025, 2025; Judek et al., 2022; Espindola; Kurka, 2026).

Table 1. **Data processing workflow**

Step1. GNSS Data Pre-processing Load GNSS data (Latitude, Longitude, Altitude, Time); Compute cumulative time vector Interpolate data for uniform temporal sampling; Compute discrete velocity;	**Step 6. GNSS Acceleration Estimation** Discrete velocity estimates (central differences); Discrete acceleration estimates: tangential and normal (centripetal); Gravity assumed constant: -9.81 m/s^2; Construction of reference acceleration vector;
Step 2. Data Purging Identify indices of data with zero velocity and/or corrupted information; Identify and remove duplicated GNSS samples;	**Step 7. IMU Data Pre-processing** Load IMU triaxial accelerometer data; Truncate IMU time to match GNSS duration; Resample IMU time to uniform step; Sampling rate reduction (decimation) to approximate GNSS vectors data length;
Step 3. Coordinate Conversion and Distance Convert geodetic WGS84 system to local cartesian; Compute cumulative linear distance;	**Step 8. IMU Synchronization and Cleaning** Mask IMU data where GNSS indicated zero velocity; Remove masked samples from interpolated IMU acceleration to match the GNSS time vector;
Step 4. Uniform Spatial Resampling Define uniform distance vector; Interpolate positions, velocities, and times as a function of distance;	**Step 9. Conditioning** Construct regression matrices for frame alignment; Estimate transformation matrix (Least Squares); Apply transformation matrix to IMU data for conditioning;
Step 5. GNSS Position Filtering Apply a low pass filter to smooth trajectory; Recalculate filtered Latitude/Longitude if necessary;	**Step 10. Error Analysis** Compare IMU raw accelerations, IMU conditioned accelerations and GNSS accelerations.

2.1. GNSS Data Management and Processing

The GNSS receiver provides geodetic primitives based on the WGS84 ellipsoid reference system. The GNSS dataset can be divided into a geodetic matrix $\mathbf{G}$ (latitude, longitude, elevation) and time-stamping vector $\boldsymbol{t}_g$, shown in Equations (1) and (2) respectively.

$$\mathbf{G} = \begin{bmatrix} latitude_0 & longitude_0 & elevation_0 \\ latitude_1 & longitude_1 & elevation_1 \\ \vdots & \vdots & \vdots \\ latitude_{N_g} & longitude_{N_g} & elevation_{N_g} \end{bmatrix}, \tag{1}$$

$$\boldsymbol{t}_g = \begin{bmatrix} t_{g_0} \\ t_{g_1} \\ \vdots \\ t_{g_{N_g}} \end{bmatrix} \tag{2}$$

where $(N_g + 1)$ is the total number of GNSS samples.

The geodetic coordinates of matrix $\mathbf{G}$, in Equation (1), are converted into cartesian coordinates system to allow kinematic analysis. The data is subsequently resampled via interpolation to ensure a uniform length distribution. The resulting spatial coordinates are defined by matrix $\mathbf{X}$ in Equation (3), while the corresponding time steps are represented by vector $\boldsymbol{t}$.

$$\mathbf{X} = \begin{bmatrix} x_0 & y_0 & z_0 \\ x_1 & y_1 & z_1 \\ \vdots & \vdots & \vdots \\ x_{N_c} & y_{N_c} & z_{N_c} \end{bmatrix} \tag{3}$$

$$\boldsymbol{t} = \begin{bmatrix} t_0 \\ t_1 \\ \vdots \\ t_{N_c} \end{bmatrix} \tag{4}$$

where $(N_c + 1)$ is the total number of cartesian interpolated samples.

2.2. Kinematic Information from GNSS Data

A numerical central differences scheme is employed to derive velocities and accelerations from the discrete positions of matrix $\mathbf{X}$. The signals are processed through a low-pass filter in order to mitigate the amplification of high-frequency positioning noise, a common side effect of numerical differentiation. This ensures that the derived kinematics of the sample reflects the low acquisition frequency of the GNSS receiver, providing a reliable baseline for IMU comparison.

Velocity estimates are computed as defined in Equation (5). This scheme employs samples that precede and proceed the desired time instant t_k, that is.

$$\boldsymbol{v}_k = \frac{\boldsymbol{x}_{k+1} - \boldsymbol{x}_{k-1}}{t_{k+1} - t_{k-1}}, k \geq 1 \tag{5}$$

where $\boldsymbol{x}_k = [x_k \quad y_k \quad z_k]$ and t_k are the vector of cartesian coordinates and time sample, respectively.

The acceleration is derived as defined in Equation (6). This numerical scheme utilizes three consecutive position samples to resolve the instantaneous acceleration.

$$\boldsymbol{a}_k = \frac{2}{t_{k+1} - t_{k-1}}\left(\frac{\boldsymbol{x}_{k+1} - \boldsymbol{x}_k}{t_{k+1} - t_k} - \frac{\boldsymbol{x}_k - \boldsymbol{x}_{k-1}}{t_k - t_{k-1}}\right), k \geq 1 \tag{6}$$

The estimated acceleration from Equation (6) is decomposed in its tangential, $\boldsymbol{a}_t$, and normal, $\boldsymbol{a}_n$, components. These are subsequently represented in the railway dynamic frame, by means of the longitudinal, a_{g_x}, lateral left, a_{g_y}, and vertical, a_{g_z}, acceleration components as shown in Figure 2. The gravitational acceleration constant, $g = 9.81\ m/s^2$, is projected in the longitudinal and vertical axis of the reference frame, according to the instantaneous gradient of the track. Consequently, Equations (7) to (99) defines the GNSS acceleration matrix, $\mathbf{A}_{GNSS}$, and vector, $\boldsymbol{a}_{GNSS}$, used for the conditioning of the IMU accelerations $\boldsymbol{a}_{IMU}$.

$$\begin{cases} \boldsymbol{a}_t = \dot{v}\hat{\boldsymbol{v}} \\ \boldsymbol{a}_n = \boldsymbol{a} - \boldsymbol{a}_t \end{cases} \rightarrow \begin{cases} a_{g_x} = \|\boldsymbol{a}_t\| - 9.81 sin(\theta_s) \\ a_{g_y} = \|\boldsymbol{a}_n\| \mathrm{sign}\big([0 \quad 0 \quad 1](\boldsymbol{v} \times \boldsymbol{a}_n)\big) \\ a_{g_z} = -g cos(\theta_s) \end{cases} \tag{7}$$

where θ_s is the instantaneous gradient defined as

$$\theta_{s_k} = \mathrm{atan}\left(\frac{z_{k+1} - z_{k-1}}{((x_{k+1} - x_{k-1})^2 + (y_{k+1} - y_{k-1})^2)^{\frac{1}{2}}}\right). \tag{8}$$

The individual vectors of estimated accelerations are grouped in a GNSS acceleration matrix defined as

$$\mathbf{A}_{GNSS} = \begin{bmatrix} \boldsymbol{a}_{GNSS_0}^{\mathsf{T}} \\ \boldsymbol{a}_{GNSS_1}^{\mathsf{T}} \\ \vdots \\ \boldsymbol{a}_{GNSS_{N_G}}^{\mathsf{T}} \end{bmatrix} \tag{9}$$

where $\boldsymbol{a}_{GNSS_k}^{\mathsf{T}} = [a_{g_{x_k}} \quad a_{g_{y_k}} \quad a_{g_{z_k}}]$ refers to the acceleration vector which is calculated at sample time t_k.

2.3. IMU Data Management

The IMU dataset provides three accelerations and at time-stamping displayed in matrix $\mathbf{A}_{IMU}$ and vector $\boldsymbol{t}_i$, respectively, as shown in Equations (10) and (11).

$$\mathbf{A}_{IMU} = \begin{bmatrix} \boldsymbol{a}_{IMU_0}^{\intercal} \\ \boldsymbol{a}_{IMU_1}^{\intercal} \\ \vdots \\ \boldsymbol{a}_{IMU_{N_G}}^{\intercal} \end{bmatrix} \tag{10}$$

$$\boldsymbol{t}_i = \begin{bmatrix} t_{i_0} \\ t_{i_1} \\ \vdots \\ t_{i_{N_i}} \end{bmatrix} \tag{11}$$

where $\boldsymbol{a}_{IMU_k}^{\intercal} = [a_{i_k} \quad a_{i_{y_k}} \quad a_{i_{z_k}}]$ refers to the acceleration vector which is calculated at sample time t_k and $(N_i + 1)$ is the total number of samples.

2.4. Spatial Synchronization and Conditioning of IMU signals

A fundamental challenge lies in the disparity between the GNSS and IMU acquisition rates. The IMU data must be filtered and decimated in order to match the GNSS time-base, ensuring that each kinematic state corresponds to a synchronized temporal observation. A decimation factor d, as defined in Equation (12), is applied to time downsample the IMU data matrix, $\mathbf{A}_{IMU}$, to the respective decimated matrix, $\mathbf{A}_{D_{IMU}}$. Following the time synchronization, a uniform trajectory-length stamping is computed to display the spatial alignment between the IMU and GNSS accelerations.

$$d = \frac{f_{IMU}}{f_{GNSS}}. \tag{12}$$

A linear transformation procedure is applied on the decimated matrix, $\mathbf{A}_{D_{IMU}}$, to align it to the estimated GNSS accelerations. The rotation, translation and scaling operations applied on the IMU accelerations samples, in order to match the GNSS acceleration estimates, are embedded in an approximated transformation matrix $\mathbf{M}$ described as

$$\mathbf{M} = \widehat{\mathbf{A}}_{GNSS}^{\intercal} \widehat{\mathbf{A}}_{D_{IMU}}^{\intercal +} \tag{13}$$

where $\widehat{\mathbf{A}}_{GNSS}^{\intercal}$ is the transposed homogenized matrix of GNSS acceleration data and $\widehat{\mathbf{A}}_{D_{IMU}}^{\intercal +}$ the transposed generalized inverse homogeneous matrix of decimated IMU accelerations.

The conditioned acceleration matrix, $\mathbf{A}_{IMU_{cond}}$, is then estimated by applying this transformation to the IMU decimated data, $\mathbf{A}_{D_{IMU}}$, effectively conditioning the IMU measurements based on the GNSS estimates. This process ensures that the two independent sensor streams represent the same physical phenomenon in a unified coordinates system.

$$\mathbf{A}_{IMU_{cond}} = \widehat{\mathbf{A}}_{D_{IMU}}\ \mathbf{M}^{\mathsf{T}} \begin{bmatrix} 1 & 0 & 0 \\ 0 & 1 & 0 \\ 0 & 0 & 1 \\ 0 & 0 & 0 \end{bmatrix} \tag{14}$$

3. EXPERIMENT AND RESULTS

The instrumentation suite utilized for data collection reflects standard industry specifications, ensuring the proposed methodology is platform-independent and adaptable to analogous architectures. The system requirements include a GNSS Receiver, capable of logging geodetic coordinates at low-frequency sampling rates ($\sim 1 - 10\ Hz$); an IMU, equipped with triaxial accelerometers featuring standard commercial dynamic ranges and high-frequency sampling (nominal $\geq 100\ Hz$); a Data Acquisition System (DAQ), equipped with synchronized logging architecture utilizing GNSS time-stamping to ensure temporal alignment and minimize inter-sensor latency. The GNSS and IMU sampling frequencies at the dataset are, respectively, $f_{GNSS} = 1\ Hz$ and $f_{IMU} = 500\ Hz$.

The proposed signal processing methodology, shown in Section 2, evaluates IMU acceleration conditioning it against GNSS estimated accelerations. The validation utilizes a representative dataset, based on a typical railway track segment. The railway track from the dataset spans a $10\ km$ path as shown in Figure 1.

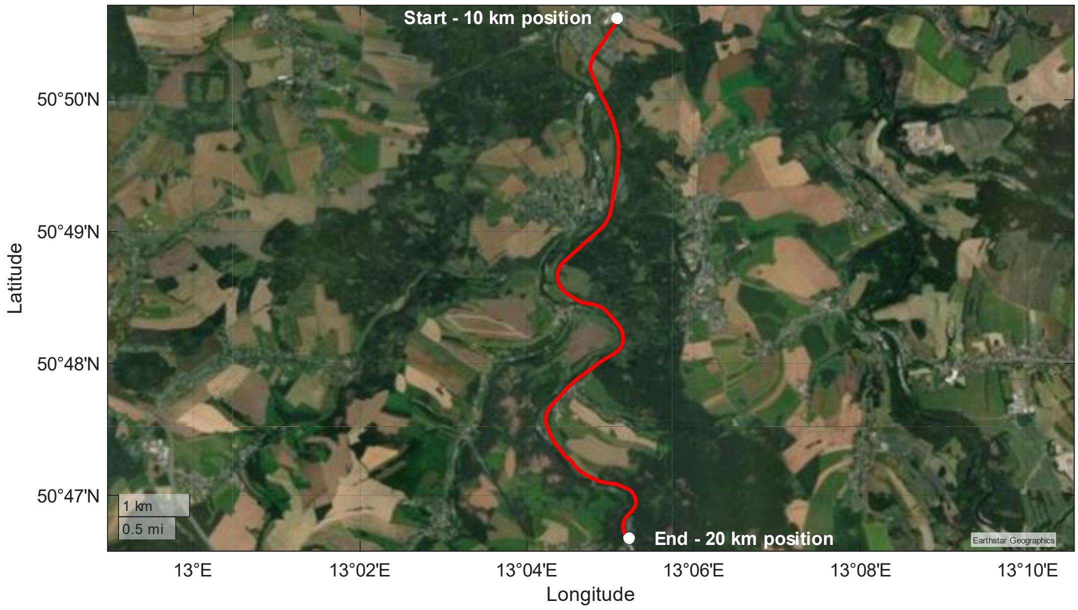

Figure 1. Railway path

Figure 2 illustrates the references frame systems adopted for GNSS and IMU measurements. The GNSS dynamic frame is defined according to SAE J670e (SAE, 2022) and ISO 8855 (ISO, 2011) standards. The IMU frame is generally not parallel to the GNSS one, and it varies arbitrarily according to the manufacturer of the measurement system.

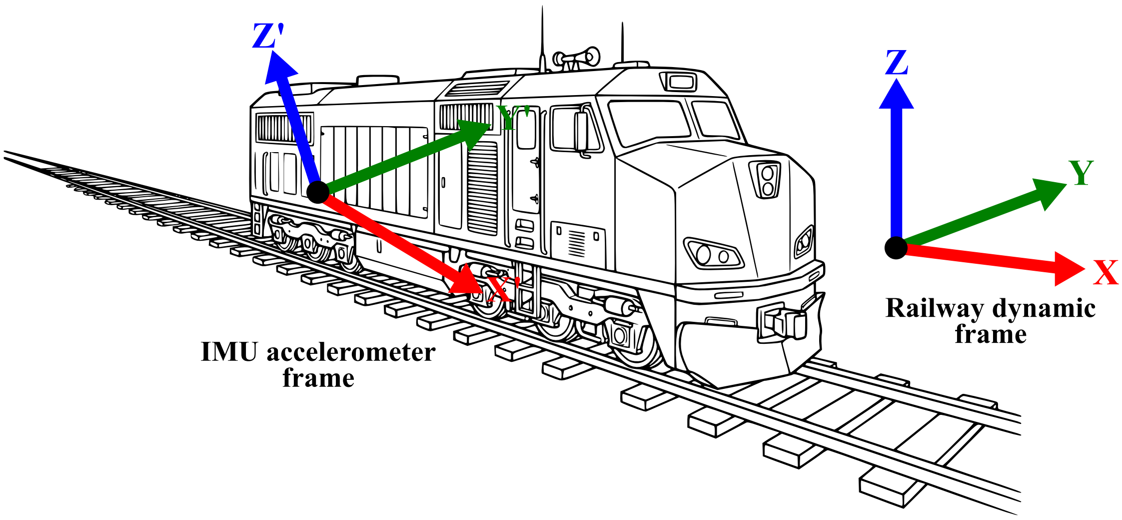

Figure 2. Frames of references

Figure 3 presents the filtered decimation results of raw IMU acceleration signals in the Y (lateral) direction. This resampling approach is designed to minimize information loss while enhancing numerical stability, offering greater reliability compared to simple downsampling.

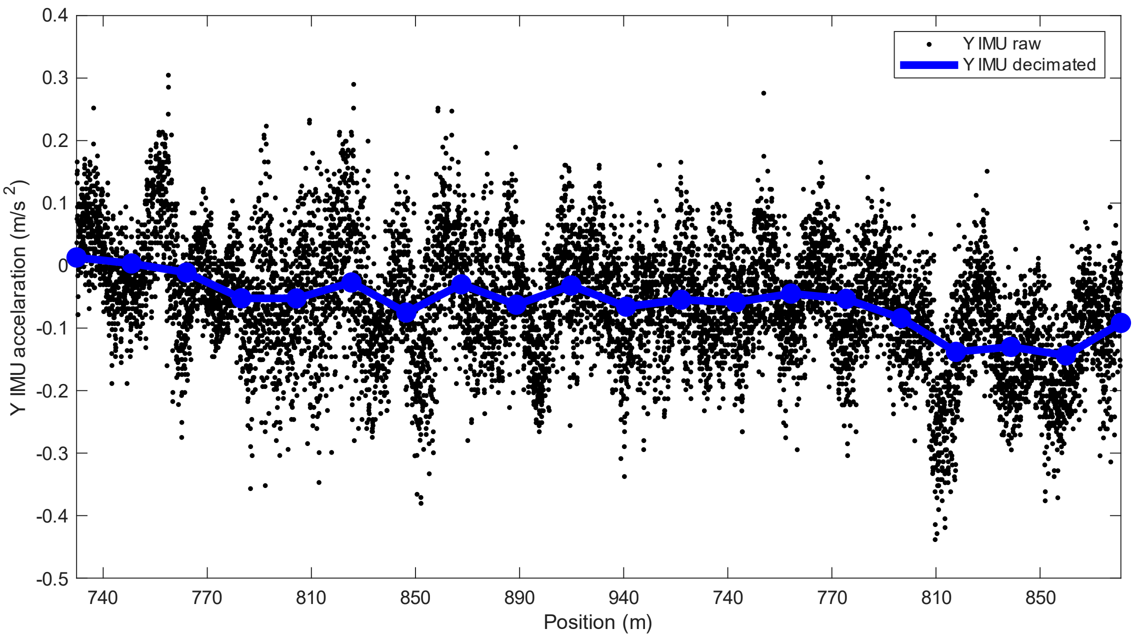

Figure 3. Decimation result of IMU Y accelerometer

Figure 4 shows the comparisons of IMU raw, IMU conditioned and GNSS accelerations across X, Y, and Z axes along the path shown on Figure 1. The left column displays raw IMU accelerations and the right column shows the same information after conditioning, both compared with GNSS accelerations.

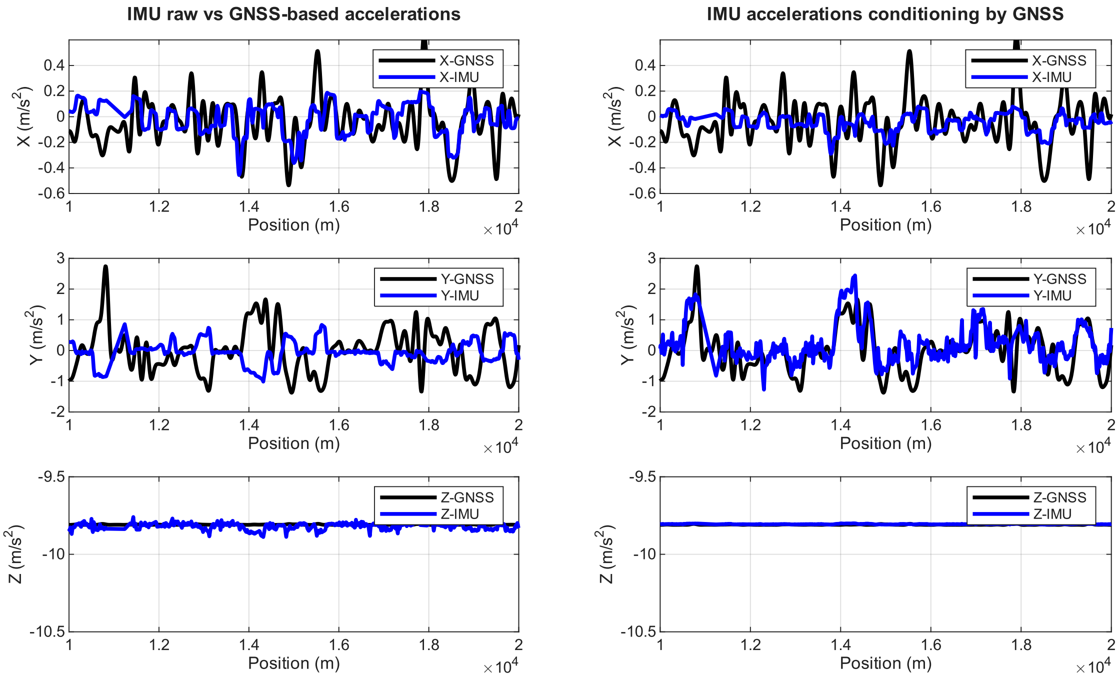

Figure 4. Comparison of IMU raw, IMU conditioning and GNSS accelerations

The results in Table 1 provide a quantitative comparison between the conditioned and unconditioned accelerations signals displayed in Figure 4. RMS values of difference between GNSS calculated and IMU measurements are displayed on the lines of the table.

Table 1. RMS values of differences of acceleration estimates.

directions	$\left\Vert \boldsymbol{a}^{\intercal}_{IMU_{cond}} - \boldsymbol{a}^{\intercal}_{GNSS} \right\Vert$ **before conditioning** $(\boldsymbol{m/s^2})$	$\left\Vert \boldsymbol{a}^{\intercal}_{IMU_{cond}} - \boldsymbol{a}^{\intercal}_{GNSS} \right\Vert$ **after conditioning** $(\boldsymbol{m/s^2})$
x	0.213850	0.2090600
y	1.175700	0.8057000
z	0.023445	0.0043447

Figure 5, displays a colormap of the IMU Y acceleration overlaid on the trajectory map. This visualization validates the physical relationship between the path's curvature and the measured normal acceleration. Positive and negative Y accelerations correspond to left and right curves, respectively.

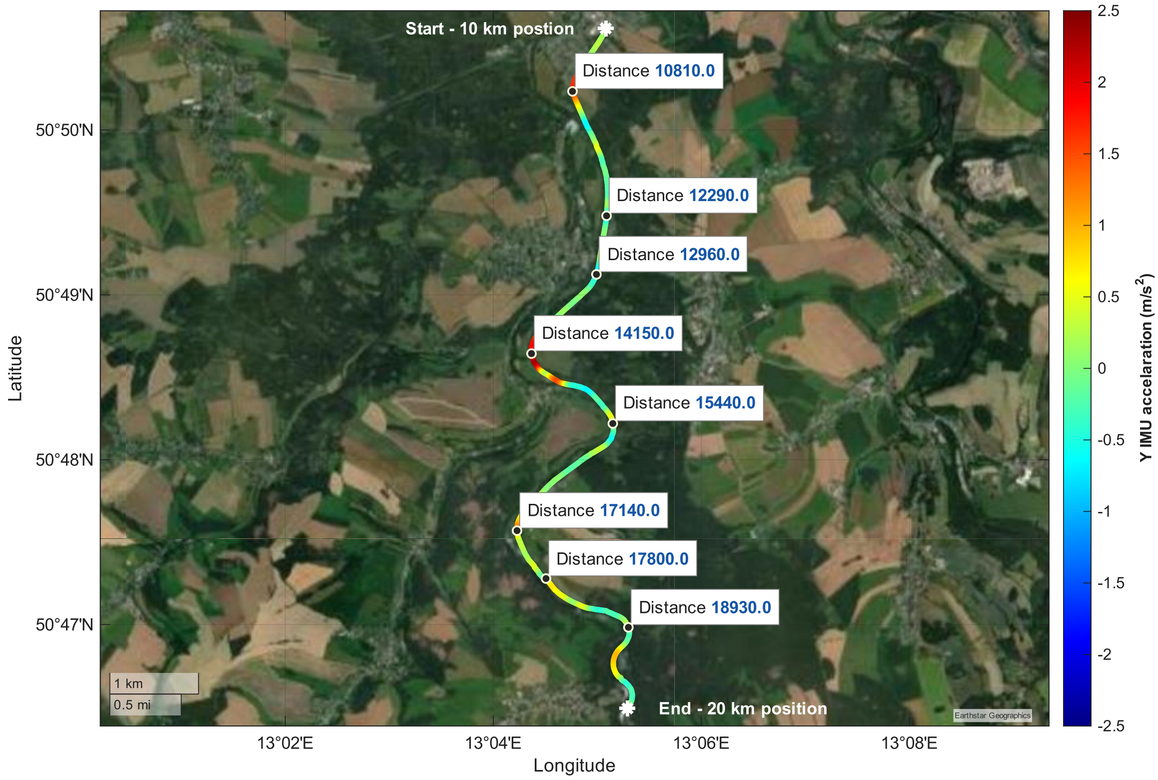

Figure 5. IMU Y acceleration conditioned over trajectory map

3.1. COMMENTS OF RESULTS

It can be observed in Figure 3 that the process of conditioned decimation of the IMU signals is essential to obtain acceleration results that are comparable to the estimated accelerations from the GNSS data.

It is important to note that the GNSS acceleration estimates are suitable to reproduce expected values in the longitudinal, lateral and vertical traveling directions, including the effect of gravity influences in the longitudinal and vertical directions in the presence of gradients. The presence of railway cant (superelevation) or vehicle rolling during curves, may also cause the gravity to influence the acceleration values in the lateral direction. The influence of such movements, however, cannot be estimated from GNSS trajectory point measurements.

The left side of Figure 4 makes it evident that IMU signals are not readily comparable to GNSS estimates due to the fact that the sensors are seldom aligned with the vehicle or the track. It can also be observed that gain amplitude and offset of the acceleration sensors may not have uniformly the same values in the X, Y and Z directions. A conditioned rotation, scale factor correction and offset displacement is therefore applied to the IMU signals in order to yield kinematic data that is coherent with the expected physical conditions defined by the geometry of the track and vehicle operational behavior.

The right side of Figure 4 shows that the conditioned IMU signals are now adherent to the expected GNSS estimates, yielding data that can be easily compared and analyzed. Conditioned IMU accelerations provide information about local instantaneous behavior of the traveling vehicle.

Table 1 indicates that the conditioned IMU signals exhibit closer agreement with the GNSS estimates, showing smaller discrepancies compared to the unconditioned signals.

Figure 5 illustrates the spatial distribution of lateral IMU accelerations along the rail corridor. The data confirms a high degree of consistency in both the magnitude and orientation of acceleration across left and right curves, aligning with expected curvature profiles. However, the analysis also reveals localized lateral acceleration spikes within nominally tangent (straight) sections. These anomalies likely indicate subtle track geometry irregularities. From a maintenance perspective, these deviations serve as critical points of interest, as they may signal emerging defects that require operational monitoring or corrective intervention.

4. CONCLUSION

This study presents a deterministic signal conditioning framework for the integration of GNSS and IMU data within railway environments, validated via a case study using an open-access experimental dataset. By leveraging kinematic derivations and linear transformations, the proposed methodology successfully reconciles disparate sampling rates and coordinate reference frames.

Furthermore, the results demonstrate that spatial alignment offers a high-fidelity alternative for sensor synchronization. This approach bypasses the need for "black-box" computational models, thereby preserving the fundamental physical phase relationship between position and acceleration.

Future research will focus on developing robust metrics for the statistical evaluation of conditioning performance. Additionally, extending this framework to multi-sensor fusion architectures will support the creation of high-reliability databases for advanced railway diagnostic analysis.

5. ACKNOWLEDGEMENTS

The authors express their gratitude to the School of Mechanical Engineering (FEM) at the University of Campinas (UNICAMP) for providing the facilities and institutional support essential to this research. Additionally, the lead author acknowledges the Federal Institute of São Paulo (IFSP) for the doctoral scholarship and financial support that made this work possible.

6. BIBLIOGRAPHY

CHEN, Qijin *et al.* Railway Track Irregularity Measuring by GNSS/INS Integration. **NAVIGATION**, v. 62, n. 1, p. 83–93, 2015. DOI: 10.1002/navi.78.

CHEN, Qijin *et al.* A Railway Track Geometry Measuring Trolley System Based on Aided INS. **Sensors**, v. 18, n. 2, p. 538, 10 fev. 2018. . DOI: 10.3390/s18020538.

ESPINDOLA, M. F.; KURKA, P. R. G. Analysis and Correlation of Railway Measurement Data Using Global Navigation Satellite System Based Curvature Estimations (accepted for presentation). *In*: EURODINAME III - INTERNATIONAL SYMPOSIUM ON DYNAMIC PROBLEMS OF MECHANICS. Gies (FR): jun. 2026.

GONZÁLEZ-CARBAJAL, J. *et al.* **Estimation of the trajectory and attitude of railway vehicles using inertial sensors with application to track geometry measurement**, 14 mar. 2022. DOI: 10.48550/arXiv.2203.07278.

HADJ-MABROUK, Habib. Contributions and limitations of AI and machine learning in railway operations, maintenance, and safety: A literature review. **Proceedings of the Institution of Mechanical Engineers, Part O: Journal of Risk and Reliability**, v. 240, n. 1, p. 3–36, 1 fev. 2026. DOI: 10.1177/1748006X251364324

ISO. **ISO 8855:2011(en) Road vehicles — Vehicle dynamics and road-holding ability — Vocabulary**. ISO - International Organization for Standardization, 2011. DOI: 10.3403/30172382.

JUDEK, Slawomir *et al.* Preparatory Railway Track Geometry Estimation Based on GNSS and IMU Systems. **Remote Sensing**, v. 14, n. 21, p. 5472, jan. 2022. DOI: 10.3390/rs14215472.

KUMAR, Muneendra. World geodetic system 1984: A modern and accurate global reference frame. **Marine Geodesy**, v. 12, n. 2, p. 117–126, 1988. DOI: 10.1080/15210608809379580.

ORBÁN, Zsolt László; GOCICA, Marius Romulus; MĂRCULESCU, Laurentiu. Study of the railway curves geometry under the effect of rail traffic over time. *In*: 7TH INTERNATIONAL CONFERENCE ON ROAD AND RAIL INFRASTRUCTURE. 2024. DOI: 10.5592/CO/cetra.2022.1459.

PIRES, Arthur; SANTOS, Guilherme Fabiano Mendonça dos; JUNIOR, Auteliano Antunes dos Santos. The Role of Data Quality for Instrumented Railway Vehicle Data. 2023. DOI: 10.17648/sef-2023-165738.

SAE. **Vehicle Dynamics Terminology**. SAE International, 2022. DOI: 10.4271/J670_202206.

WINTER, Hanno. Rail Vehicle Positioning Data Set: Lucy, October 2018. 27 nov. 2020. DOI: 10.25534/tudatalib-360.

XIE, Rong; CHEN, Chunjun. Optimized Detection Algorithm for Vertical Irregularities in Vertical Curve Segments. **Applied Sciences**, v. 14, n. 22, p. 10753, jan. 2024. DOI: 10.3390/app142210753.

YALINIZ, Polat; İÇA, Sezgin. Evaluation of the Track Geometry Quality with Standard Deviation Method and Quality Indices: Case study of Kütahya-Afyonkarahisar Railway Line, v. 20, n. 6, p. 1068–1078, 31 dez. 2020. DOI: 10.35414/akufemubid.684336.

ZHOU, Y.; YANG, Y.; HECHT, M. Real-time predication of railway track curvature using gyroscope and GPS sensors, out. 2023. DOI: 10.1109/ISS58390.2023.10361925

ZHOU, Yichang *et al.* Estimating railway track curvature using gyroscope and GPS sensors. **Scientific Reports**, v.15, n.1, p.8037, 2025. DOI: 10.1038/s41598-025-91255-x.